Supplementary Information

Nanotechnological immunoassay for rapid label-free analysis of candidate malaria vaccines

Giulio Brunetti[§1], Francesco Padovani[§1,2], Annalisa De Pastina[1], Chiara Rotella[1], Amy Monahan[1], Stephen L. Hoffman[3], Said A. Jongo[4], Salim Abdulla[4], Giampietro Corradin[5], Gerd Pluschke[6,8], Claudia Daubenberger[7,8] and Martin Hegner*[1]*

[1] Centre for Research on Adaptive Nanostructures and Nanodevices (CRANN), School of Physics, Trinity College Dublin, Dublin, Ireland;

[2] Institute of Functional Epigenetics, Helmholtz Zentrum München (HMGU), Neuherberg 85764, Germany

[3] Sanaria Inc., Rockville MD, USA

[4] Bagamoyo Research and Training Centre, Ifakara Health Institute, Bagamoyo, Tanzania

[5] Biochemistry Department, University of Lausanne, Epalinges, Switzerland

[6] Medical Parasitology and Infection Biology Department, Molecular Immunology Unit, Swiss Tropical and Public Health Institute, Basel, Switzerland

[7] Medical Parasitology and Infection Biology Department, Clinical Immunology Unit, Swiss Tropical and Public Health Institute, Basel, Switzerland

[8] University of Basel, Switzerland

* Corresponding authors: hegnerm@tcd.ie; claudia.daubenberger@swisstph.ch;

§ These authors contributed equally to this work

Data acquisition via PLL

As can be found in several previous publications [1-7], the standard method to detect the mechanical response of cantilever sensors in our group consists in carrying out a frequency sweep and extracting the resonance frequency by fitting the obtained amplitude spectra. However, in this manuscript, some datasets (see main text Fig. 5b) are obtained via a newly implemented strategy: a phase locked loop (PLL) allows to directly monitor the sensors' resonance frequency over time.

A PLL is built via an in-house developed LabVIEW code, directly interfaced with the experimental hardware, and able to track up to 18 sensors in parallel (unpublished). A voltage signal $V(\omega)$ is sent to the piezo-actuator mounted under the cantilever chip to actuate the *nth* device at resonance frequency ω_n, and it is also used as reference signal. The mechanical motion of the device is captured via a position sensitive detector (PSD). The phase shift $\delta\Phi$ between driving signal (generated) and response signal (measured) is converted to a frequency shift $\delta\omega$ via a calibrated PID controller and is applied as a correction to $V(\omega)$, thus closing the feedback loop. To do so, a fine-tuned digital PID controller continuously computes an adjustment to the driving frequency that maintains the phase shift $\delta\Phi$ constant at resonance. Before each experiment, the cantilevers are mounted in the microfluidic chamber and immersed in a buffer solution to stabilize. During this equilibration step, the software computes for each cantilever the following parameters: a) the optimal phase that maximizes the resonant motion's amplitude and b) the optimal PID parameters via an autotuning algorithm.

This procedure is applied to every sensor in the array, resulting in up to 18 PLLs running sequentially and able to track up to 4 modes per cantilever: the piezoactuator excites each cantilever at its nominal resonance frequency for a short period of time (few ms), while the optical laser is sequentially focused on each sensor surface. The *n* mechanical signals collected from each sensor are separately stored and converted to $\delta\omega$ values by *n* PIDs running in parallel. The dead time between the collection of two consecutive frequency responses on the same sensor is in the order of few seconds and is mainly due to physical stage movement. Such dead time does not constitute a limitation for our experiments, as the time range of interest for biological events lies in the order of few minutes, as shown in this manuscript. Data collected via PLL (main text Fig. 5b) show a frequency noise reduction of more than one order of magnitude with respect to the frequency sweep acquisition method (main text Fig.

5a, c). Frequency noise of single sensors is evaluated by calculating the Allan Deviation of the frequency signals over time (Fig. S1) and multiplying them for the respective tracked resonance frequencies (~380 kHz, in this example). Evaluating the noise in the frequency is paramount, as this is directly proportional to the mass resolution of cantilever sensors [8]. Given the reduction by more than 1 order of magnitude in frequency noise (Table S1), we expect the same improvement in terms of mass resolution of our sensors when signals are detected via PLL method (data not published).

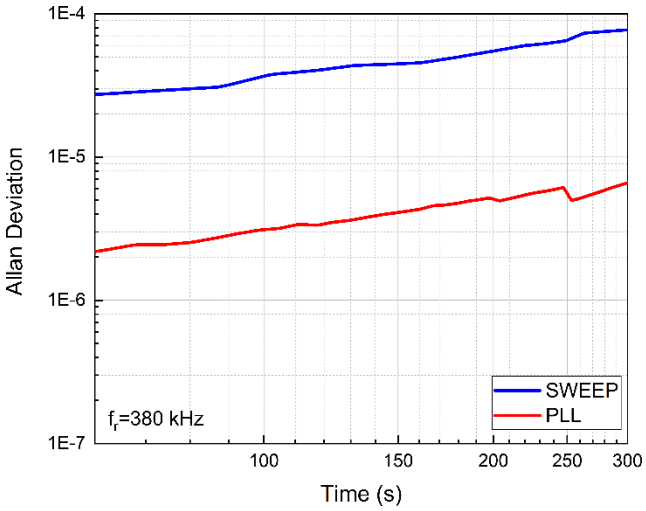

Figure S1 - Allan deviation plots obtained from the frequency signals over time collected via frequency sweep (blue) and PLL (red) method. Each line is the average Allan Deviation of the 8 individual sensors in the array. Both the plots scale as $\tau^{0.8}$, indicating that in this integration time range the main noise contribution is given by the thermal drift in the system. PLL-obtained Allan deviation is lower than the sweep-obtained one by a factor 12, resulting in an expected mass resolution improved by the same factor.

Table S1 - Allan deviation (AD) and Frequency noise (f noise) calculated from Fig. 2, considering an integration time of 5 minutes (relevant time range for biological events and for our experimental timeline). An estimation of the mass resolution is also provided, by taking into account the resonator mass (≈150 ng).

	SWEEP	**PLL**
AD@300s	$8x10^{-5}$	$6x10^{-6}$
f noise @300s	≈30 Hz	≈2.3 Hz
Estimated mass resolution @300s	11.8 pg	0.9 pg

The noise analysis of the measurements in Fig. 6 (main text) provides a measure for the noise floor/mass resolution of the presented peak tracking measurements. As indicated here in Fig. S2, the differential mass noise in the serum experiments is in the order of ~4 -19 pg with the frequency sweep approach (Table S2). This is improved by factor 10 when PLL tracking is applied as explained in the previous paragraph (see Fig. 5b, main text).

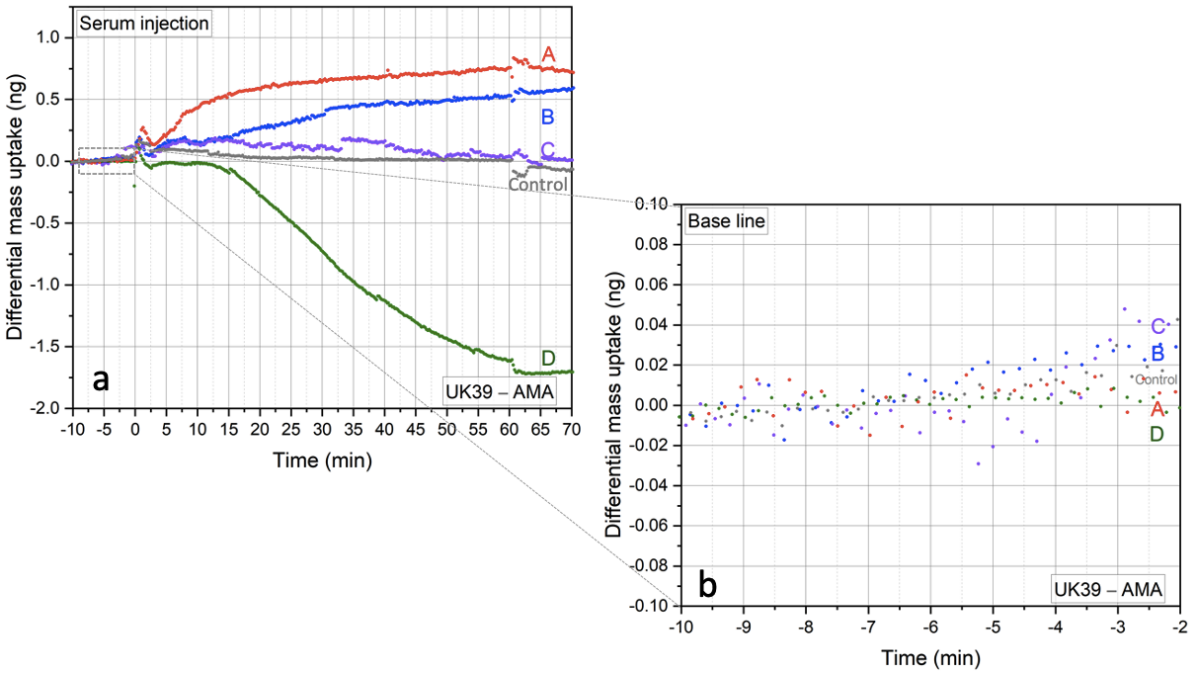

Figure S2 - Immunogenic response of 5 adult volunteers' serum samples from the BSPZV 1 clinical trial. (Left - a): Sanaria PfSPZ Vaccine serum analysis. Four sensors are functionalised with the AMA49-C1 and four with UK39 peptidomimetics. Their frequency sweep responses are group averaged, subtracted from the AMA response and plotted. (Right - b) Zoom into the baseline time period before the injection of the serum samples to allow analysis of the noise in the cantilever array experiment. The mass noise is ranging from ~4 to 19 pg (Table S2).

Table S2 - Mass noise analysis utilising the frequency sweep method in an 8-minute period from -10 to -2 minutes before injection of serum samples.

	N	Average (pg)	Std. Dev. (pg)
A	33	3.7	8.0
B	34	10.2	13.5
C	36	1.6	18.6
D	40	1.3	3.6
Control	35	5.3	11.3
Average		4.4	11.0

ELISA and nanomechanical dose response curves

ELISA analysis with peptide-PE conjugates were performed essentially as briefly described in ref.[9]. Polysorp plates (Nunc; Fisher Scientific, Wohlen, Switzerland) were coated overnight at 4°C with 100 µl of a 10 µg/ml solution of UK39 in PBS (pH 7.2). After three washings with PBS containing 0.05% Tween 20, wells were blocked with 5% milk powder in PBS for 30 min at 37°C and washed three times again. Plates were then incubated with serial PBS dilutions of anti-peptide mAbs in hybridoma supernatant (~1 µg/ml) containing 0.05% Tween 20 and 0.5% milk powder for 2 hr at 37°C. Estimating a single digit percentage content of specific mAbs against the UK39 epitope in the supernatant. After washing, plates were incubated with alkaline phosphatase-conjugated goat anti-mouse IgG (Fc-specific) antibodies (Sigma, St. Louis, MO) for 1 hr at 37°C. After washing again, a phosphatase substrate solution (1 mg/ml *p*-nitrophenyl phosphate [Sigma] in a pH 9.8 buffer solution containing 10% [v/v] diethanolamine and 0.02% $MgCl_2$) was added and the plates were incubated in the dark at room temperature until the colorimetric reaction had progressed sufficiently. The optical density was measured at 405 nm on a Titertek Multiscan MCC/340 reader (Labsystems, Helsinki, Finland).

The cantilever dose-response curves were measured using protein A purified mAbs EP9. In order to be comparable with ELISA, a volume of 60 µl was injected for each separate experiment and the samples were diluted in PBS, following routine ELISA procedure.

Fig. S3b shows the direct comparison of the hybridoma supernatant mAbs ELISA response to the cantilever array measurement (value obtained from the sum of 4 cantilevers each (UK39-AMA49-C1)). Fig. S3 is the result of 8 independent experiments, each conducted with a separate array of 8 individually functionalised sensors. For each sensor, three resonance modes have been tracked simultaneously as standard procedure internal control. A total number of 192 parallel measurement points is indeed represented over time compared with the ELISA output of averaged single end-point measurements. Both methods show similar sensitivity and level out at ~ 150pg/ml.

Cantilever array mass measurements (noise ~1pg) are limited by the mass transported to the liquid chamber [10]. Increasing the injection volume of the cantilever measurements would allow to measure lower concentrations per ml.

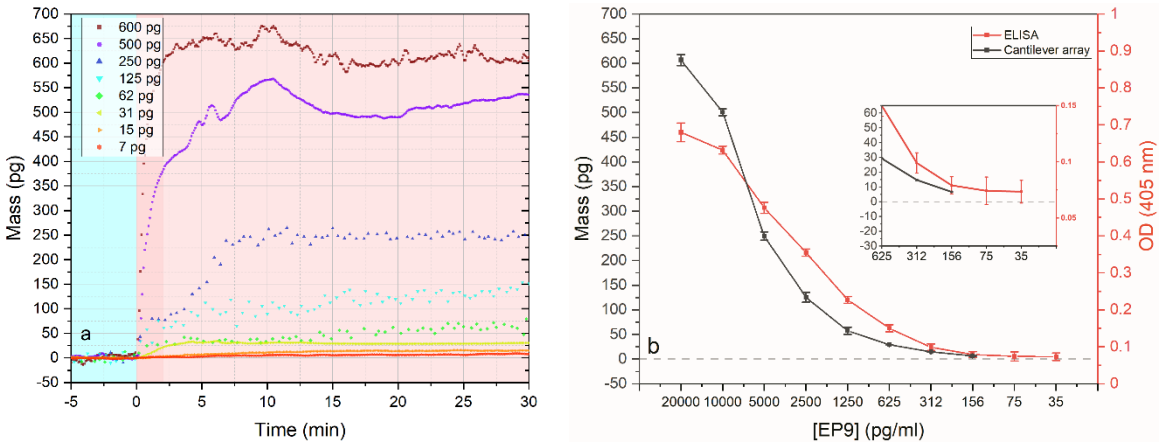

Figure S3: Comparison of dose-response curves of cantilever-based bioassay and ELISA. a: EP9 mass detection (pg) in individual serial dilutions of anti-UK39 mAb EP9 versus time. Four cantilevers were functionalized with AMA49-C1 and four sensors with UK39 and injections of anti-UK39 EP9 antibodies were carried out. A dilution ratio of 1:1 in PBS was applied in each step starting from 20 ng/ml EP9 mAbs to ~156 pg/ml. Each sensor response represents an independent experiment where the sensors' responses were compared by subtracting the sum in terms of mass absorption of the two sets of 4 cantilevers (differential read-out, UK39/AMA49-C1). Signals in dark blue, light blue and green were analysed by resonance frequency tracking via frequency sweep method. Meanwhile, the newly implemented approach (phase locked loop method, discussed above in the supplementary information) has been used to carry out the remaining five experiments, further reducing the frequency noise by a factor 10. **b: Direct comparison of dose-response curves of ELISA and cantilever-based bioassay**. Response to serial dilutions of the cantilever-based array (black) and the ELISA assay (red), both performed with diluted EP9 mAbs. Cantilever-based values were taken at 20 minutes and their standard

deviation obtained by extrapolating the values between 15 and 25 minutes of each experiment. The cantilever specific standard deviation was calculated considering the average of 2 x 4 sensors. The ELISA dilution series was conducted in hybridoma supernatant. For additional details see our data from ref. [9]. Inset: Zoom to low concentration range.

Differential nanomechanical measurements

In most ELISA tests the individual assays are designed by physisorbing receptor proteins or antibodies to non-treated polystyrene surfaces of microtiter plates through passive adsorption [11]. These plates are provided with different surface properties ranging in hydrophobicity and charge [12, 13]. Hydrophobic interfaces may partially denature proteins that bind to it [14]. In order to maintain its folding and consequent 3D structure, soluble proteins orient the hydrophobic amino acids towards its core and the polar and charged amino acids against the surrounding solution and ions [15]. When a soluble protein binds to a hydrophobic surface, this is facilitated by partially orienting its internal hydrophobic amino acids against the surface to become more hydrophobic. This way the surface binding energy is maximized. Proteins that are folding secondary and tertiary structures can be partially denatured in this process and great care has to be taken to minimize the effect [16, 17].

The residual sequence and properties are crucial to anchor specific epitopes to the assays. Indeed, on high-binding hydrophobic ELISA plates [11], alanines within alpha helical structures will be oriented towards the polystyrene surface, which can hamper the correctly folded structure in protein loops. In contrast, on nanomechanical sensors the malaria vaccine candidates with the PE-peptidomimetics [9, 18, 19] were coupled via lysine's residuals or primary amines to a self-assembled monolayer that becomes hydrophilic after conversion. The coupling is providing a pin-point covalent attachment [16, 20]. Proteins that are bound this way retain their 3D folding better, since solutions and ions have three-dimensional access. In more detail, UK39, exhibits several alanines that are more likely to be located inwards (away from H_2O) in the properly folded loop [9] and one primary amine for covalent coupling. AMA49-C1 exposes 4 lysines and one primary amine [18, 19] to allow covalent coupling to the NHS-activated DSU self-assembled monolayers (Fig. 1).

The binding of vesicle membranes integrated with delicate membrane receptors to DSU monolayers also proved favorably for the subsequent nanomechanical analysis [2]. The

membrane protein did not lose its integrity. Specific binding of T4 phages to the embedded FhuA receptors, anchored at their NH_2 containing residues, could be demonstrated and verified image via SEM imaging [2].

We would define this direct coupling to an amino reactive surface bound monolayer as an "active immobilization", in contrast to the passive immobilization on high-bind ELISA plates. Indeed, depending on how the ELISA sandwich assay is designed, the proteins or antibodies that act as receptors for diagnostic targets, are passively bound to the surface.

In a classic ELISA test, the ELISA reaction would correspond to the AMA – HSA analysis in a differential nanomechanical read-out (main text, Fig. 5).

In an optimized nanomechanical differential assay, the chemical, topographic, polar, charged 'structure' of a sensor receptor interface of a sensor used as a reference, should mimic the actual molecular epitope as best as possible. Therefore, the assay should allow to distinguish specifically between the peptidomimetics PE-UK39 and PE-AMA49-C1 only.

After the peptides are covalently bound to the sensor's functionalized DSU monolayers, the whole PE-amino acids epitopes are presented to the fluid. Upon differential readout, all interactions that occur at the hydrophobic end or at the phosphatidyl-ethanolamine are subtracted and only the interactions at the peptide loops are measured as the purely peptide-specific recognition pattern.

When using HSA on the sensor surface as a reference, there are several additional epitopes available, apart from the targeted ones. In fact, HSA has to denature slightly when being physisorbed, and can be bound to by different molecules in serum. Such detection on the surface has nothing to do with UK39. Even if a decrease in binding is noticed, as in the case of HSA passivation on ELISA surfaces, some recognition patterns can be attributed to serum proteins including immunoglobulins.

Since we are interested in the pure signal towards UK39 or AMA49-C1, it is better to decorate the reference sensors of each assay with PE-UK39 (if one wants to measure AMA49-C1) or PE-AMA49-C1 (if one wants to measure UK39).

A schematic of the differential nanomechanical measurement is represented in Fig. S4.

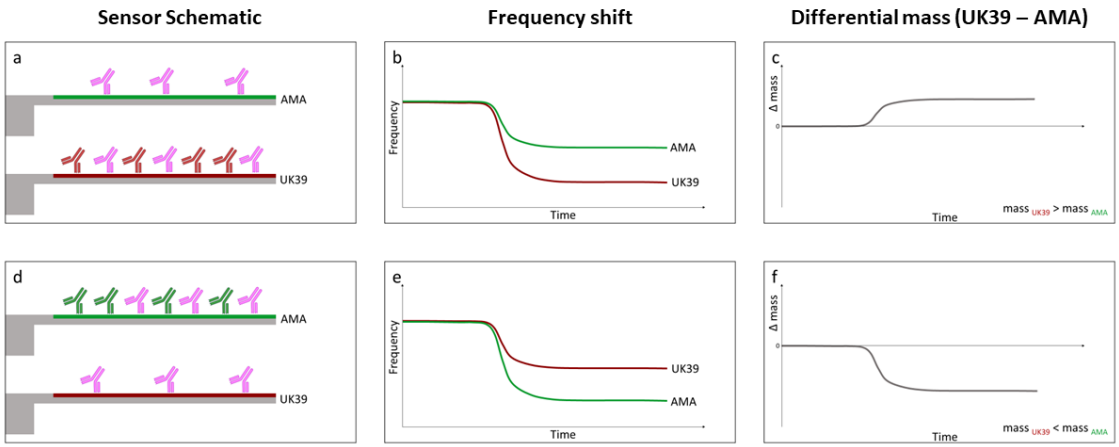

Figure S4 - Differential mass assay. Schematic of two cantilevers functionalized with AMA (green) and UK39 (red) peptides (panels a, d). The epitope-specific antibody recognition (green antibodies towards AMA, red antibodies towards UK39 and pink antibodies as unspecific interactions) generates a frequency shift based on the different sensor functionalisations (panels b, e). Taking the characteristics of the fluid around the sensors and the sensors' dimensions into account, the frequency shifts are converted into a mass addition towards one or the other epitope (panels c, f) [1].

This direct comparison in one well is not possible on an ELISA plate, where the remaining surfaces besides the antigen-receptor will be passivated as much as possible with HSA, in order to avoid unspecific interactions. Recognition patterns for polyclonal antibodies that are rather at the phosphatidyl-ethanolamine amino acid chain transition, or at the transition to the hydrophobic anchor, remain.

The PE-peptidomimetic could also be non-ideally integrated in the virosome (this is not shown in the cartoon chemistry Fig. 1) and thus influence a part of the immunization. With only HSA as a reference, interactions that are not specifically related to the UK39 (or AMA49-C1) peptide can result. This can lead to an overestimation or an underestimation of the actual signal. This effect can only be evaluated when the surfaces in a measurement are directly compared *in-situ*. Comparing the result of UK39 – AMA49-C1 allows to measure the tendency caused by the surface property and not by the antigenic epitopes. This is not possible with ELISA, where individual wells have separate functionalization. Once the first antibody or antigen is bound, the secondary antibody in the ELISA assay cannot differentiate whether primary layer antibodies are bound to UK39 or to a different epitope. This is normally optimized during the ELISA assay validation in order to minimize such effects.

In nanomechanical assays we cannot exclude, by measuring masses bound in liquid on one sensor only, whether they are strictly related to the diagnostic target or other proteins.

Therefore, the contribution to the signal based on molecular recognition absolutely requires therefore differential analysis. It is better to utilize receptor layers that are overall similar, but differ slightly in the molecular recognition pattern. This is key to the resulting mass difference in UK39 – AMA49-C1 (AMA) (see Fig. S5). Furthermore, all environmental effects (e.g. temperature or viscosity changes) are subtracted [21-23].

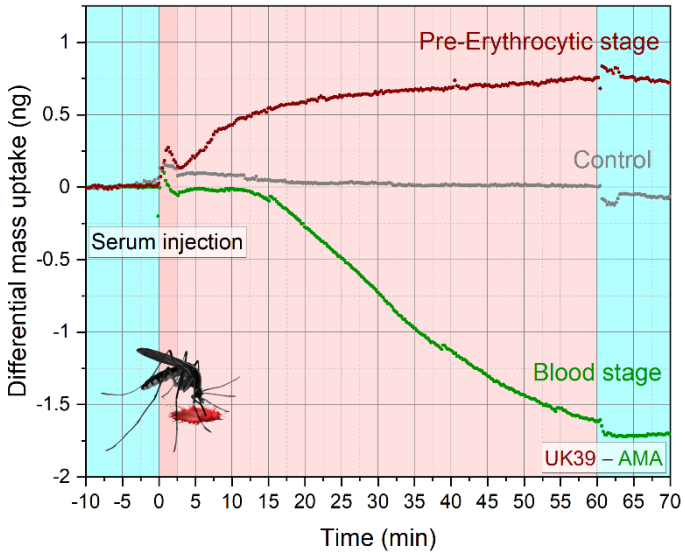

Figure S5 - Immunogenic response of adult volunteers' serum samples from Fig. 6. Differential read-out allows direct discrimination between the two human malaria mosquito transmitted disease stages – the pre-erythrocytic and the blood stage.

References

1. T. Braun, V. Barwich, M. K. Ghatkesar, A. H. Bredekamp, C. Gerber, M. Hegner and H. P. Lang, *Phys. Rev. E.*, 2005, **72**, 031907.
2. T. Braun, M. K. Ghatkesar, N. Backmann, W. Grange, P. Boulanger, L. Letellier, H.-P. Lang, A. Bietsch, C. Gerber and M. Hegner, *Nat. Nanotechnol.*, 2009, **4**, 179.
3. K. Y. Gfeller, N. Nugaeva and M. Hegner, *Appl. Environ. Microbiol.*, 2005, **71**, 2626-2631.
4. N. Maloney, G. Lukacs, J. Jensen and M. Hegner, *Nanoscale*, 2014, **6**, 8242-8249.
5. F. Padovani, J. Duffy and M. Hegner, *Anal. Chem.*, 2016, **89**, 751-758.
6. F. Padovani, J. Duffy and M. Hegner, *Nanoscale*, 2017, **9**, 17939-17947.
7. M. Walther, P. M. Fleming, F. Padovani and M. Hegner, *EPJ Tech. Instrum.*, 2015, **2**, 7.
8. S. Schmid, L. G. Villanueva and M. L. Roukes, *Fundamentals of Nanomechanical Resonators*, Springer International Publishing, 2016.
9. S. L. Okitsu, U. Kienzl, K. Moehle, O. Silvie, E. Peduzzi, M. S. Mueller, R. W. Sauerwein, H. Matile, R. Zurbriggen and D. Mazier, *Chem. Biol.*, 2007, **14**, 577-587.
10. J. L. Arlett, E. B. Myers and M. L. Roukes, *Nat. Nanotechnol.*, 2011, **6**, 203-215.
11. J. Tan, B. K. Sack, D. Oyen, I. Zenklusen, L. Piccoli, S. Barbieri, M. Foglierini, C. S. Fregni, J. Marcandalli, S. Jongo, S. Abdulla, L. Perez, G. Corradin, L. Varani, F. Sallusto, B. K. L. Sim, S. L. Hoffman, S. H. I. Kappe, C. Daubenberger, I. A. Wilson and A. Lanzavecchia, *Nat. Med.*, 2018, **24**, 401.

12. A. B. Bergeron, C. J. Bortz and A. Rossi, Corning Medium and High Binding ELISA Microplates for Select Target Size Binding Assays, https://www.corning.com/media/worldwide/cls/documents/applications/CLS-AN-497%20DL.pdf).
13. P. Esser, Thermo Scientifc Solid Phase Guide, https://assets.thermofisher.com/TFS-Assets/LCD/Scientific-Resources/Thermo_Scientific_Solid_Phase_Guide.pdf, 2020).
14. H. Thurow and K. Geisen, *Diabetologia*, 1984, **2**, 212-218.
15. K. A. Dill, S. B. Ozkan, M. S. Shell and T. R. Weikl, *Annual Review of Biophysics*, 2008, **37**, 289-316.
16. A. S. Hoffmann and J. A. Hubbell, in *Biomaterials Science: An Introduction to Materials in Medicine*, eds. B. Ratner, A. Hoffman, F. Schoen and J. Lemons, Academic Press/Elsevier, London, San Diego, 2004, vol. 2nd Edition, pp. 225 - 237.
17. B. Rathner and A. S. Hoffman, in *Biomaterials Science: An Introduction to Materials in Medicine*, eds. B. Ratner, A. Hoffman, F. Schoen and J. Lemons, Academic Press/Elsevier, London, San Diego, 2004, vol. 2nd Edition, pp. 197 - 201.
18. M. S. Mueller, A. Renard, F. Boato, D. Vogel, M. Naegeli, R. Zurbriggen, J. A. Robinson and G. Pluschke, *Infect Immun*, 2003, **71**, 4749-4758.
19. B. Pfeiffer, E. Peduzzi, K. Moehle, R. Zurbriggen, R. Glück, G. Pluschke and J. Robinson, *Angew. Chem. Int. Ed.*, 2003, **42**, 2368 - 2371.
20. P. Wagner, M. Hegner, P. Kernen, F. Zaugg and G. Semenza, *Biophys. J.*, 1996, **70**, 2052-2066.
21. H. P. Lang, M. Hegner and C. Gerber, in *Appl. Scan. Probe Met. IV - Ind. Appl., B*, ed. H. F. Bhushan, Springer Verlag, Berlin, New York, Heidelberg, 2006.
22. H. P. Lang, M. Hegner and C. Gerber, *Materials today*, 2005, **8**, 30-36.
23. J. Duffy, F. Padovani, G. Brunetti, P. Noy, U. Certa and M. Hegner, *Nanoscale*, 2018, **10**, 12797-12804.